

The Infrared Continuum Sizes of Be Star Disks

Y. Touhami, D. R. Gies

Center for High Angular Resolution Astronomy and Department of Physics and Astronomy, Georgia State University, P. O. Box 4106, Atlanta, GA 30302-4106; yamina@chara.gsu.edu, gies@chara.gsu.edu

G. H. Schaefer

Georgia State University, CHARA Array, P. O. Box 48, Mount Wilson, CA 91023; schaefer@chara-array.org

ABSTRACT

We present an analysis of the near-infrared continuum emission from the circumstellar gas disks of Be stars using a radiative transfer code for a parametrized version of the viscous decretion disk model. This isothermal gas model creates predicted images that we use to estimate the HWHM emission radius along the major axis of the projected disk and the spatially integrated flux excess at wavelengths of 1.7, 2.1, 4.8, 9, and 18 μm . We discuss in detail the effect of the disk base density, inclination angle, stellar effective temperature, and other physical parameters on the derived disk sizes and color excesses. We calculate color excess estimates relative to the stellar V -band flux for a sample of 130 Be stars using photometry from 2MASS and the AKARI infrared camera all-sky survey. The color excess relations from our models make a good match of the observed color excesses of Be stars. We also present our results on the projected size of the disk as a function of wavelength for the classical Be star ζ Tauri, and we show that the model predictions are consistent with interferometric observations in the H , K' , and 12 μm bands.

Subject headings: stars: emission-line, Be — circumstellar matter — infrared: stars — stars: individual (ζ Tau)

1. Introduction

Be stars are rapidly rotating B-type stars that at times host a circumstellar gas disk (Porter & Rivinius 2003). They exhibit various observational attributes such as photospheric

non-radial pulsations, hydrogen and iron emission lines that are formed in the disk, infrared, millimeter, and radio continuum excess emission from the disk, intrinsic linear polarization from electron scattering in the disk, and, in an increasing number of cases, the presence of a compact companion (Struve 1931; Slettebak 1988; Porter & Rivinius 2003). The circumstellar ionized gas around Be stars gives rise to a large infrared excess emission that is seen in their spectral energy distribution. Observations conducted by Woolf et al. (1970) at $10\ \mu\text{m}$ were the first to suggest that the IR excess of Be stars is due to free-free and bound-free emission and not due to thermal dust emission. An early study by Gehrz et al. (1974) confirmed that the large IR emission detected from 33 Be stars originates in the free-free emission only and that thermal dust emission fails to reproduce the observations at $20\ \mu\text{m}$. The IR excess from ionized disk gas was subsequently investigated with space-based data from IRAS (Coté & Waters 1987; Waters et al. 1987; Dougherty et al. 1994), ISO (Waters et al. 2000), and MSX (Clarke et al. 2005), and with ground-based mid-IR (Rinehart et al. 1999) and near-IR data from the 2MASS survey (Zhang et al. 2005). The near- and mid-IR excess flux emission is known to increase with wavelength and to dominate over the stellar flux at long wavelengths. Observations probing the circumstellar disk structure at many wavelengths and across all Be spectral types are necessary to understand the complex physical processes involving disk formation.

Models of the disk continuum emission have become increasingly comprehensive in recent years. Some of the first models that assumed a simple geometry and gas density distribution (Waters 1986; Kastner & Mazzali 1989; Dougherty et al. 1994; Rinehart et al. 1999) were successful in fitting the color excesses in many cases. A significant improvement came with the development of the viscous decretion disk model (Lee et al. 1991; Porter 1999; Okazaki 2001) in which the gas orbits with nearly-Keplerian velocity, but with a small radial outflow motion caused by turbulent viscosity. These models characterize the disk density with a radial power law, $\rho \propto R^{-3.5}$, and a vertical extension set by hydrostatic equilibrium. The IR-excesses predicted are similar to those observed, but often require a density exponent with smaller absolute value and/or a non-isothermal temperature distribution in order to match observations (Porter 1999, 2003). Recent models include radiation processes in the disk and determine fully consistent temperature and density distributions (Carciofi & Bjorkman 2006; Jones et al. 2008), and these are remarkably successful in explaining the continuum and line emission in some Be stars (Carciofi et al. 2006; Halonen et al. 2008).

The advent of optical long baseline interferometry has now led to the direct resolution of Be star disks in both emission lines (Quirrenbach et al. 1997; Stee & Bittar 2001; Tycner et al. 2006; Meilland et al. 2007; Carciofi et al. 2009) and in the IR-continuum (Gies et al. 2007; Meilland et al. 2007, 2009). These observations offer us the means to explore the geometry of Be disks and to measure the disk gas temperature. Since the IR-excess flux depends

mainly on the projected size of the disk and the gas surface brightness (from the temperature dependent source function), a comparison of the angular size and flux excess provides a way to investigate the disk-to-star temperature ratio and (in principle) to study spatial temperature variations in the disk.

Our goal in this paper is to explore the IR-excess flux predictions for a parametrized version of the isothermal, viscous disk model that we have developed to study CHARA Array K' -band observations of Be disks (Gies et al. 2007). We calculate the near-IR color excesses for various representative stellar and disk parameters and compare these with new IR measurements from the AKARI satellite (Ita et al. 2010). In §2, we describe the model in detail and discuss how the different physical parameters of the model influence the color excess. In §3, we discuss the color-color diagrams and compare our results to the AKARI all-sky survey observations of Be stars. Finally in §4, we consider the example of the Be star ζ Tau, and we show that the predicted variation of circumstellar disk angular size with wavelength is consistent with the available multi-wavelength observations.

2. Be Star Circumstellar Disk Models

Our original model (Gies et al. 2007) created images of Be stars and their disks for comparison with K' -band interferometry from the GSU CHARA Array. In order to investigate the disk emission over a range of wavelengths in the near and mid-IR, we have extended the model to calculate the disk flux distribution at 1.66 (H -band), 2.13 (K' -band), 4.8, 9, and 18 μm . Our code is a realization of an isothermal viscous decretion disk model. In brief, the gas density distribution is given by

$$\rho(R, Z) = \rho_0 R^{-n} \exp \left[-\frac{1}{2} \left(\frac{Z}{H(R)} \right)^2 \right] \quad (1)$$

where R and Z are the radial and the vertical cylindrical coordinates, respectively, in units of stellar radii, ρ_0 is the gas base density, and n is the radial density exponent. $H(R)$ is the disk vertical scale height defined by

$$H(R) = \frac{c_s}{V_K} R^{3/2} \quad (2)$$

where c_s is the sound speed (in turn dependent on the disk gas temperature) and V_K is the Keplerian velocity at the stellar equator. Our multi-wavelength disk model has four physical parameters: the base density ρ_0 , the density exponent n , the disk-to-star temperature ratio T_d/T_{eff} , and the outer boundary disk radius R_{out} . There are also two observational parameters: the wavelength λ and the inclination angle i .

The code follows the method of Hummel & Vrancken (2000) and solves the equation of transfer along a grid of sight-lines around the star and disk. The result is a spatial image of the system (see examples in Gies et al. 2007). We assume source functions equal to the Planck functions for the temperatures of the star and disk. The disk optical depth in the near-IR is mainly due to free-free and bound-free processes, and it can be expressed using an incremental step ds along a projected rectilinear coordinate grid as follows

$$d\tau = C(\lambda, T_d)\rho(R, Z)^2 ds \quad (3)$$

where the coefficient $C(\lambda, T_d)$ is given by equation (5) in Dougherty et al. (1994). This coefficient includes terms for the Gaunt factors for bound-free and free-free emission. We set these Gaunt factors by interpolating in wavelength in the tables from Waters & Lamers (1984). For simplicity, we estimate the ionization equilibrium and Gaunt factors throughout the disk for two idealized cases (adopted from Lamers & Waters 1984 and Waters & Lamers 1984): (1) a hot plasma with ionized H, singly ionized He, and doubly ionized C, N, O for disk temperatures above 15000 K, and (2) a warm plasma consisting of ionized H, neutral He, and singly ionized C, N, and O for lower temperatures. Note that we ignore the electron scattering flux in the model, since this flux source is proportional to the stellar flux and hence is relatively small at longer wavelengths.

Here we focus on two results of the calculation, the flux excess and apparent disk size. We determine from the derived image the total monochromatic flux of the star and disk, F_{total} , and then we estimate the net disk contribution as $F_d = F_{\text{total}} - F_s$, i.e., the net flux relative to the unobscured star. We show this quantity in a magnitude form of flux excess as $E^*(V^* - m_\lambda) = 2.5 \log(1 + F_d/F_s)$. This notation is based upon the assumption that the disk contribution is negligible in the optical V -band, so that we can write the flux excess as how many magnitudes brighter the system appears at longer wavelengths where the disk shines brightly. This latter assumption should be taken with caution. In fact, there is ample evidence from the V -band brightening of Be stars during their active phases that the disks do contribute to the V -band (perhaps by as much as 50%) in those cases with dense and large circumstellar disks. Consequently, by referring the colors to a V magnitude that is brighter than that for the star alone, the observed color excesses may be lower than the calculated color excesses in some cases. The star superscript is used here to differentiate this type of “reddening” or color-excess from the kind normally associated with interstellar extinction. Waters (1986) expresses the monochromatic flux excess as $Z = F_{\text{total}}/F_s$, so in our notation $E^*(V^* - m_\lambda) = 2.5 \log Z$. We also use the calculated spatial image of the star plus disk to find the HWHM of the emission envelope along the projected major axis of the disk, and we define an effective, observational disk radius R_d/R_s as the ratio of the angular HWHM to the angular stellar radius.

We begin by showing our results on the flux excess and disk size for a default model, and then we show how changes in the physical and observational parameters affect the results. In the default model, we assume that the central star is an early-type star with effective temperature $T_{\text{eff}} = 30$ kK, radius $R_s/R_\odot = 10$, and mass $M_s/M_\odot = 15.5$. The infrared excesses derived from observations suggest that the power-law density exponent of the circumstellar disk falls in the range $n \approx 2.0$ to 3.5 (Coté & Waters 1987; Waters et al. 1987), so we assumed $n = 3$ here, a value consistent with our prior interferometric results (Gies et al. 2007). The other adopted parameters for the default model are a disk-to-star temperature ratio $T_d/T_{\text{eff}} = 2/3$, an outer boundary disk radius $R_{\text{out}}/R_s = 21.4$, and an inclination angle $i = 45^\circ$. These parameters are selected from an earlier model for the Be star γ Cas (Gies et al. 2007), and the outer boundary, for example, corresponds to the Roche radius of this binary system. Our results for the color excess and disk radius are listed in Table 1 as a function of waveband and base density for this model and several others described below.

We show in Figure 1 how the color excesses $E^*(V^* - K)$, $E^*(V^* - 9\mu\text{m})$, and $E^*(V^* - 18\mu\text{m})$ vary as a function of the disk base density ρ_0 . The disk flux excess is highly dependent on density ρ_0 and wavelength λ . The color excesses at low densities are insignificant because the disk is optically thin in the continuum and the stellar photospheric flux dominates. As the density increases, the color excess resulting from the disk emission becomes more important and dominates at longer wavelengths. In fact, the excess emission at $18\mu\text{m}$ is higher than at $9\mu\text{m}$ and at $2.13\mu\text{m}$ because the optically thick-thin boundary of the disk becomes bigger and the excess flux larger at longer wavelengths.

The relationship between the $18\mu\text{m}$ color excess and apparent disk emission radius for the default model is shown as a solid line in Figure 2 (for $T_d/T_{\text{eff}} = 2/3$). We also show a number of other models where different parameters are varied in turn. The case with a higher inclination angle $i = 80^\circ$ is plotted with a dashed line. As the inclination increases, the projected disk surface area decreases and hence the disk flux excess also declines. However, at higher inclination, a ray through the outer part of the disk encounters significant density over a longer path, and the increased optical depth causes the effective radius to appear larger. Consequently, as the inclination increases, points on the default model curve are shifted to lower color excess and higher effective radius.

Changes in the other parameters have less influence on the size – color excess relation shown in Figure 2. For example, for the case of a cooler Be star with an effective temperature of $T_{\text{eff}} = 15$ kK (shown by the dashed-dotted line), the resulting color excess and disk radius are almost identical to that for the default case ($T_{\text{eff}} = 30$ kK; solid line) at all values of the disk base density. This is due to the temperature dependence of the optical depth coefficient,

$C(\lambda, T_d) \propto T_d^{-1/2}$. The radius of the optically thick-thin boundary will vary with this optical depth term, and the source function is proportional to temperature in the Rayleigh-Jeans part of the spectrum. Thus, the disk emission flux will vary as the product of projected area and source function, or $\sim R_d^2 S \sim (T_d^{-1/2})^2 T_d$, which is approximately constant, all other parameters being equal.

If we adopt a smaller value of the outer radius of the disk ($R_{\text{out}}/R_s = 14.6$; shown by the dash-triple dotted line), we see that there is no difference between this case and the default case ($R_{\text{out}}/R_s = 21.6$) at low densities. It is only at very high density that the truncation of the outer disk leads to a slight decline in the color excess.

Finally, the dotted line shows the influence of our choice of disk temperature. In the default model, we adopt an isothermal disk with a temperature of $T_d = 2/3 T_{\text{eff}}$ following the example of Hummel & Vrancken (2000). We compare in Figure 2 the color excess for two disk temperatures, $1/2 T_{\text{eff}}$ and $2/3 T_{\text{eff}}$. The source function varies approximately linearly with disk temperature T_d , so a drop of 25% in disk temperature will create a comparable decrease in emission flux (for a given disk radius). This decrease of ≈ 0.3 mag in $E^*(V^* - 18\mu\text{m})$ is seen in Figure 2 at the high density end where the disk flux dominates. This suggests that coordinated interferometric and IR excess observations are potentially an important means to study the disk temperature properties, especially for Be stars with dense and large disks.

Our results show many similarities to the color excesses derived by Dougherty et al. (1994) from a much simpler model. They confined the emitting gas to a wedge-like disk with a density law dependent only on the distance to the star, and they solved the radiative transfer problem for just $i = 0$ and $i = 90^\circ$. Dougherty et al. (1994) also investigated the dependence of the near-IR color excess on the model parameters, but they present relative color excesses between adjacent near-IR bands ($CE(J-K)$ and $CE(K-L)$; see their Fig. 7) rather than referencing the excess to the stellar V -band flux as we do here. Nevertheless, the agreement is reasonable, and, for example, their expression for the disk optically thick-thin boundary as a power law function of wavelength and base density (their eq. 7) is similar to our results for R_d/R_s in Table 1. Furthermore, Dougherty et al. (1994) also presented instructive results for a range in the density power law exponent, with values greater and less than the $n = 3$ value assumed here (they used the symbol β for the density exponent). Their work showed that a smaller n yields a more spatially extended disk and consequently larger color excesses.

Recent models for Be star disks present detailed calculations of the gas temperature as a function of disk position. Carciofi & Bjorkman (2006) solve for the temperature distribution in the disk through a Monte-Carlo treatment of radiative transfer, and they find that gas temperature reaches $T_d \approx 0.6 T_{\text{eff}}$ in optically thin parts of the disk in one rep-

representative model. Sigut et al. (2009) present results for a grid of models that maintain hydrostatic equilibrium with the spatial variations in temperature, and they find that the density averaged temperature is $T_d \approx 0.6T_{\text{eff}}$, however, this average temperature declines with increasing disk density (perhaps by 20 – 30%; see their Fig. 8). Their models indicate that the temperatures tend to be cooler in the denser regions closer to the star and in the mid-plane. The IR-excesses calculated from such models are similar to those for isothermal models. For example, Carciofi & Bjorkman (2006) show that the predicted flux excesses for different inclination angles are almost the same for the isothermal and non-isothermal model they study (see the upper panel of their Fig. 10). However, since the disk gas temperatures decline with increasing density, we suspect that a plot like Figure 2 of color excess and radius for such fully consistent, non-isothermal models would look similar to our $T_d = 2/3T_{\text{eff}}$ curve at small excess (low density), but would tend towards the $T_d = 1/2T_{\text{eff}}$ curve at large excess (high density).

3. AKARI IR Fluxes of Be Stars

With the recent release of the AKARI/IRC mid-infrared all-sky survey (Ishihara et al. 2010), we now have the opportunity to compare the observed and model flux excesses at 9 and 18 μm . We took as our sample 130 Be stars from the work of Dougherty et al. (1994) that have reliable estimates of interstellar reddening $E(B-V)$. We then collected V , K_s , $m(9\mu\text{m})$, and $m(18\mu\text{m})$ magnitudes from Ita et al. (2010) for each target. The V magnitudes were taken from the SIMBAD database, K_s magnitudes from 2MASS (Skrutskie et al. 2006), and $m(9\mu\text{m})$ and $m(18\mu\text{m})$ magnitudes from AKARI. These last two are based on the Vega magnitude scale, where a model spectrum by R. L. Kurucz defines the flux zero point as a function of wavelength (Tanabé et al. 2008). The photometry we use here was collected at different times, and since Be stars are inherently variable (Porter & Rivinius 2003), some scatter must be expected in the results because the flux excesses will change with disk density variations. We also collected stellar effective temperatures for each target from the work of Frémat et al. (2005) in order to estimate the intrinsic stellar colors.

Our goal is to determine a flux excess by comparing the observed and intrinsic stellar colors of the targets. Using the same magnitude notation given in the previous section, we determine the near-IR flux excesses by

$$E^*(V^* - m_\lambda) = V - m_\lambda - E(B - V) \times (3.10 - R_\lambda) - (V - m_\lambda)(\text{Kurucz})$$

where the ratio of interstellar extinction to reddening is $R_\lambda = A_\lambda/E(B - V)$ (Fitzpatrick 1999) and $(V - m_\lambda)(\text{Kurucz})$ is the intrinsic stellar color derived from monochromatic sampling of flux ratios of model spectra with the Vega spectrum from R. L. Kurucz. These

model spectra are also from Kurucz atmospheres for solar metallicity, gravity $\log g = 4.0$, and a microturbulent velocity of 2 km s^{-1} (parameters appropriate for main sequence B-stars). The intrinsic colors are listed in Table 2 as a function of effective temperature T_{eff} , and we found that they made a reliable match to the AKARI colors of B-stars with known T_{eff} from interferometry and bolometric luminosity (Code et al. 1976). The derived color excesses for the Be stars are listed in Table 3. The typical errors in the AKARI magnitudes are $\pm 0.05 \text{ mag}$, but they can be larger for the 2MASS K_s magnitudes since many of the Be stars are bright and their magnitudes were determined from the wings of the point spread function. We caution that the intrinsic colors from Table 2 may not be appropriate in some cases because rotational gravity darkening will make stars with large inclination appear redder (although the color difference may be negated if opaque disk gas blocks the cooler equatorial zones from view). We have ignored these complications because they are difficult to estimate accurately and because these colors are not too sensitive to temperature for hot stars.

We plot the results in two color-color diagrams in Figures 3 and 4. These show the flux excesses at 9 and $18 \mu\text{m}$, respectively, as a function of the K_s -band excess. Also shown in these figures are plots of our model near-IR excesses (§2) for the default model and cases with differing stellar temperature and disk inclination. All these models make similar predictions about color-color excesses, and they appear to match the observations well, especially if allowance is made for the slight negative shift in observed colors caused by our neglect of disk flux in the V -band. There are three objects plotted in Figures 3 and 4 with $E^*(V^* - K) \approx 1.0$ that fall well below the predicted trends. All three are binary stars in which the companion is a K-giant (HD 45910 = AX Mon, Elias et al. 1997; HD 50123 = HZ CMa, Sterken et al. 1994; HD 50820, Ginestet & Carquillat 2002), and we suspect that their relatively large brightness in K_s is due to the flux from the cool giant companion. Otherwise, the overall agreement suggests that the viscous decretion disk model provides a satisfactory description of the near-IR flux excesses.

Inspection of Figures 3 and 4 shows that at the high density limit, the color-color excess diagrams assume a linear form. This part of the relation occurs when the disk flux dominates over the stellar flux and the colors become those of the disk. Thus, we expect that all Be stars will appear with approximately the same near-IR color for those cases with sufficiently dense disks. As an example, we show in Figure 5 a near-IR color-magnitude diagram for all those sample stars with Hipparcos parallax data yielding absolute magnitude errors less than 0.5 mag (van Leeuwen 2007). This plot shows the interstellar extinction corrected, absolute K_s magnitude versus an interstellar reddening corrected, color index $K_s - m(9 \mu\text{m})$ (shown as plus signs). Each of these is connected by a dotted line to a color and magnitude coordinate corresponding to one with the derived color excess removed (nominally for the

star itself; shown as diamonds). Also plotted is the zero-age main-sequence (left dashed line) from the work of Lejeune & Schaerer (2001) that was formed from the theoretical (T_{eff}, V) track and the colors in Table 2 for $T_{\text{eff}} = 10 - 30$ kK. From Figure 3, the asymptotic form of the excess relation is

$$E^*(V^* - 9 \mu\text{m}) \approx E^*(V^* - K_s) + 1.35$$

and we also plot the main-sequence translated in color by this expression and brighter in K_s by 1 magnitude (see Fig. 1) to represent the approximate positions of the dense disk case (right dashed line). We see that the Be stars appear over a range in color between the no disk and strong disk cases, with many of the Be stars having colors close to the strong disk limit. This diagram is similar in appearance to that for the Be stars discovered in the LMC by Bonanos et al. (2010), who present a plot in the $(J - [3.6\mu\text{m}], J)$ plane.

4. Angular Size of the Disk of ζ Tau

Meilland et al. (2009) measured some of the first Be disk diameters at 8 and 12 μm using the VLTI and MIDI instrument. Their results suggested that the disk sizes do not increase with wavelength as predicted by simple models. For example, they found that the angular size of the disk of the Be star α Ara was approximately constant between 2 and 12 μm , and they speculated that the disks may be truncated by the tidal effects of a binary companion. Our models and those of Dougherty et al. (1994) suggest that the color excesses and effective radii could reach finite limits in those cases with high disk density and a small outer boundary.

Here we demonstrate that at least for one case, ζ Tau, the angular size variation with wavelength is consistent with model predictions. The Be star ζ Tau (HD 37202, HR 1910, HIP 26451) is a frequently observed target with a strong IR-excess (Touhami et al. 2010). The $\text{H}\alpha$ emission line in its spectrum shows cyclic V/R variations on a timescale of few years, which are explained by the presence of a one-armed oscillation in its circumstellar disk (Okazaki et al. 2002; Carciofi et al. 2009). The star is the primary in a spectroscopic binary with an orbital period of $P = 133$ d (Ruždjak et al. 2009). The system is composed of a $11M_{\odot}$ primary Be type star and a $1.3M_{\odot}$ secondary star (Floquet et al. 1989). Several interferometric studies of the $\text{H}\alpha$ emission line (Quirrenbach et al. 1997; Tycner et al. 2004) and the IR-continuum (Gies et al. 2007; Carciofi et al. 2009; Meilland et al. 2009) have resolved the circumstellar disk around the primary Be star. A recent CHARA Array investigation by Schaefer et al. (2010) shows that the disk of ζ Tau is viewed almost edge-on and that the disk may be precessing with the V/R cycle.

We used our model to estimate R_d/R_s for ζ Tau over the wavelength range of 1.7 –

18 μm . We adopted the stellar parameters from Gies et al. (2007): mass $M_s = 11.2M_\odot$, radius $R_s = 5.5R_\odot$, effective temperature $T_{\text{eff}} = 19 \text{ kK}$, and parallax $\pi = 7.82 \text{ mas}$. The disk parameters assumed are $\rho_0 = 1.4 \times 10^{-10} \text{ g cm}^{-3}$, $n = 2.9$, $i = 87^\circ$, and $T_d/T_{\text{eff}} = 2/3$ (based on fits of recent K' observations with the CHARA Array). The outer disk boundary was set at the binary Roche radius, $R_{\text{out}} = R_{\text{Roche}} = 146R_\odot$. We then determined the disk effective radius over the wavelength grid, and our results for R_d/R_s are plotted in Figure 6.

In order to test our model predictions, we collected recent interferometric measurements of the angular size of ζ Tau. We start with the two CHARA Array results. The weighted average of the H -band, Gaussian FWHM from Schaefer et al. (2010) is $1.61 \pm 0.05 \text{ mas}$, and the corresponding K' -band value is $1.79 \pm 0.07 \text{ mas}$ (Gies et al. 2007). The target was also observed at longer wavelengths with VLTI/MIDI by Meilland et al. (2009). They found an upper limit of FWHM less than 2.6 mas at 8 μm , but they resolved the disk at 12 μm and found a FWHM = $5.7 \pm 2.2 \text{ mas}$. These estimates are over-plotted for comparison on the theoretical dotted-line shown in Figure 6 by assuming a stellar, limb darkened, angular diameter of $\theta_{LD} = 0.40 \pm 0.04 \text{ mas}$. We find that the size of the emitting region does increase with increasing wavelength in a manner mostly consistent with the observations. The 8 μm upper limit falls slightly below the model curve in Figure 6, but we suspect that this difference is marginal given the fact that the VLTI/MIDI observations were not made at an optimal position angle for the disk’s orientation in the sky. Thus, we suggest that the viscous decretion disk predictions about disk size as a function of wavelength pass the test for the case of ζ Tau. However, it is certainly possible that disk truncation effects will be more important in binary Be stars with smaller semimajor axes.

We are currently completing a survey of bright, northern sky, Be stars with the CHARA Array in the K' -band, and we plan to use our model to fit both the angular diameters and flux excesses. Since the flux excess depends on the angular size and source function, we will be able to infer the source function and hence disk temperature for a diverse sample of Be stars. We also intend to compare the H and K' -band diameters for a subset of Be stars with CHARA MIRC observations (Schaefer et al. 2010).

This material is based on work supported by the National Science Foundation under Grant AST-0606861. YT thanks the NASA Georgia Space Grant Consortium for a fellowship. Institutional support has been provided from the GSU College of Arts and Sciences and from the Research Program Enhancement fund of the Board of Regents of the University System of Georgia, administered through the GSU Office of the Vice President for Research. We gratefully acknowledge all this support.

Facility: CHARA

REFERENCES

- Bonanos, A. Z., et al. 2010, *AJ*, 140, 416
- Carciofi, A. C., & Bjorkman, J. E. 2006, *ApJ*, 639, 1081
- Carciofi, A. C., Okazaki, A. T., le Bouquin, J.-B., Štefl, S., Rivinius, T., Baade, D., Bjorkman, J. E., & Hummel, C. A. 2009, *A&A*, 504, 915
- Carciofi, A. C., et al. 2006, *ApJ*, 652, 1617
- Clarke, A. J., Oudmaijer, R. D., & Lumsden, S. L. 2005, *MNRAS*, 363, 1111
- Code, A. D., Bless, R. C., Davis, J., & Brown, R. H. 1976, *ApJ*, 203, 417
- Coté, J., & Waters, L. B. F. M. 1987, *A&A*, 176, 93
- Dougherty, S. M., Waters, L. B. F. M., Burki, G., Coté, J., Cramer, N., van Kerkwijk, M. H., & Taylor, A. R. 1994, *A&A*, 290, 609
- Elias, N. M., II, et al. 1997, *ApJ*, 484, 394
- Fitzpatrick, E. L. 1999, *PASP*, 111, 63
- Floquet, M., Hubert, A. M., Maillard, J. P., Chauville, J., & Chatzichristou, H. 1989, *A&A*, 214, 295
- Frémat, Y., Zorec, J., Hubert, A.-M., & Floquet, M. 2005, *A&A*, 440, 305
- Gehrz, R. D., Hackwell, J. A., & Jones, T. W., 1974, *ApJ*, 191, 675
- Gies, D. R., et al. 2007, *ApJ*, 654, 527
- Ginestet, N., & Carquillat, J. M. 2002, *ApJS*, 143, 513
- Halonen, R. J., et al. 2008, *PASP*, 120, 498
- Hummel, W., & Vrancken, M. 2000, *A&A*, 359, 1075
- Ishihara, D., et al. 2010, *A&A*, 514, A1
- Ita, Y., et al. 2010, *A&A*, 514, A2
- Jones, C. E., Sigut, T. A. A., & Porter, J. M. 2008, *MNRAS*, 386, 1922
- Kastner, J. H., & Mazzali, P. A., 1989, *A&A*, 210, 295

- Lamers, H. J. G. L. M., & Waters, L. B. F. M. 1984, *A&A*, 136, 37
- Lee, U., Osaki, Y., & Saio, H. 1991, *A&A*, 244, L5
- Lejeune, T., & Schaerer, D. 2001, *A&A*, 366, 538
- Meilland, A., Stee, P., Chesneau, O., & Jones, C. 2009, *A&A*, 505, 687
- Meilland, A., et al. 2007, *A&A*, 464, 59
- Okazaki, A. T. 2001, *PASJ*, 53, 119
- Okazaki, A. T., Bate, M. R., Ogilvie, G. I., & Pringle, J. E. 2002. *MNRAS*, 337, 967
- Porter, J. M. 1999, *A&A*, 348, 512
- Porter, J. M. 2003, *Be Star Newsl.*, 36, 6
- Porter, J. M., & Rivinius, Th. 2003, *PASP*, 115, 1153
- Quirrenbach, A., et al. 1997, *ApJ*, 479, 477
- Rinehart, S. A., Houck, J. R., & Smith, J. D. 1999, *AJ*, 118, 2974
- Ruždjak, D., et al. 2009, *A&A*, 506, 1319
- Schaefer, G. H., et al. 2010, *AJ*, 140, 1838
- Sigut, T. A., McGill, M. A., & Jones, C. E. 2009, *ApJ*, 699, 1973
- Skrutskie, M. F., et al. 2006, *AJ*, 131, 1163
- Slettebak, A. 1988, *PASP*, 100, 770
- Stee, P., & Bittar, J. 2001, *A&A*, 367, 532
- Sterken, C., Vogt, N., & Mennickent, R. 1994, *A&A*, 291, 473
- Struve, O. 1931, *ApJ*, 73, 94
- Tanabé, T., et al. 2008, *PASJ*, 60, S375
- Touhami, Y., et al. 2010, *PASP*, 122, 379
- Tycner, C., et al. 2004, *AJ*, 127, 1194
- Tycner, C., et al. 2006, *AJ*, 131, 2710

van Leeuwen, F. 2007, *A&A*, 474, 653

Waters, L. B. F. M. 1986, *A&A*, 162, 121

Waters, L. B. F. M., Côté, J., & Lamers, H. J. G. L. M. 1987, *A&A*, 185, 206

Waters, L. B. F. M., & Lamers, H. J. G. L. M. 1984, *A&AS*, 57, 327

Waters, L. B. F. M., et al. 2000, in *The Be Phenomenon in Early-Type Stars*, IAU Coll. 175 (ASP Conf. Proc. 214), ed. M. A. Smith, H. F. Henrichs, & J. Fabregat (San Francisco: ASP), 145

Woolf, N. J., Stein, W. A., & Strittmatter, P. A. 1970, *A&A*, 9, 252

Zhang, P., Chen P. S., & Yang, H. T. 2005, *NewA*, 10,325

Table 1. IR Color Excesses for Different Viscous Disk Models

Parameter	1.0×10^{-12}	5.1×10^{-12}	1.0×10^{-11}	ρ_0 (g cm $^{-3}$) 3.1×10^{-11}	8.1×10^{-11}	1.0×10^{-10}	2.0×10^{-10}
$n = 3, i = 45^\circ, T_{\text{eff}} = 30 \text{ kK}, R_{\text{out}} = 21.4 R_s, T_d = 2/3 T_{\text{eff}}$							
$E^*(V^* - H) \dots\dots$	0.02	0.03	0.06	0.29	0.91	1.08	1.65
$E^*(V^* - K) \dots\dots$	0.02	0.05	0.11	0.59	1.38	1.57	2.19
$E^*(V^* - 4.8 \mu\text{m})$	0.02	0.11	0.31	1.04	1.86	2.06	2.69
$E^*(V^* - 9 \mu\text{m}) \dots$	0.04	0.43	0.91	1.86	2.76	2.97	3.61
$E^*(V^* - 18 \mu\text{m})$	0.13	1.00	1.61	2.59	3.51	3.71	4.33
$R_d/R_s(H) \dots\dots\dots$	1.23	1.24	1.25	1.41	2.10	2.28	2.97
$R_d/R_s(K) \dots\dots\dots$	1.23	1.24	1.26	1.58	2.39	2.61	3.40
$R_d/R_s(4.8 \mu\text{m}) \dots$	1.24	1.27	1.39	2.17	3.15	3.44	4.56
$R_d/R_s(9 \mu\text{m}) \dots\dots$	1.24	1.38	1.79	2.76	4.07	4.49	6.05
$R_d/R_s(18 \mu\text{m}) \dots\dots$	1.26	1.95	2.55	3.92	5.95	6.57	8.82
$n = 3, i = 80^\circ, T_{\text{eff}} = 30 \text{ kK}, R_{\text{out}} = 21.4 R_s, T_d = 2/3 T_{\text{eff}}$							
$E^*(V^* - H) \dots\dots$	0.02	0.03	0.04	0.11	0.39	0.49	0.91
$E^*(V^* - K) \dots\dots$	0.02	0.03	0.04	0.25	0.72	0.87	1.41
$E^*(V^* - 4.8 \mu\text{m})$	0.02	0.05	0.13	0.48	1.11	1.28	1.88
$E^*(V^* - 9 \mu\text{m}) \dots$	0.03	0.19	0.43	1.11	1.95	2.15	2.78
$E^*(V^* - 18 \mu\text{m})$	0.07	0.49	0.89	1.78	2.68	2.88	3.48
$R_d/R_s(H) \dots\dots\dots$	1.24	1.26	1.31	1.83	2.77	2.95	3.99
$R_d/R_s(K) \dots\dots\dots$	1.24	1.27	1.39	2.14	3.13	3.49	4.56
$R_d/R_s(4.8 \mu\text{m}) \dots$	1.24	1.39	1.80	2.87	4.29	4.62	6.21
$R_d/R_s(9 \mu\text{m}) \dots\dots$	1.26	1.77	2.43	3.64	5.61	6.11	8.17
$R_d/R_s(18 \mu\text{m}) \dots\dots$	1.37	2.57	3.43	5.33	8.03	8.86	11.97
$n = 3, i = 45^\circ, T_{\text{eff}} = 15 \text{ kK}, R_{\text{out}} = 21.4 R_s, T_d = 2/3 T_{\text{eff}}$							
$E^*(V^* - H) \dots\dots$	0.02	0.04	0.08	0.43	1.11	1.28	1.86
$E^*(V^* - K) \dots\dots$	0.02	0.06	0.15	0.73	1.53	1.73	2.35
$E^*(V^* - 4.8 \mu\text{m})$	0.04	0.17	0.46	1.26	2.11	2.31	2.94
$E^*(V^* - 9 \mu\text{m}) \dots$	0.05	0.49	1.01	1.96	2.86	3.07	3.71
$E^*(V^* - 18 \mu\text{m})$	0.14	1.04	1.64	2.63	3.54	3.79	4.36
$R_d/R_s(H) \dots\dots\dots$	1.23	1.24	1.27	1.64	2.46	2.68	3.51
$R_d/R_s(K) \dots\dots\dots$	1.23	1.25	1.29	1.77	2.62	2.85	3.76
$R_d/R_s(4.8 \mu\text{m}) \dots$	1.24	1.30	1.55	2.44	3.59	3.94	5.23
$R_d/R_s(9 \mu\text{m}) \dots\dots$	1.24	1.52	2.04	3.12	4.63	5.12	6.86
$R_d/R_s(18 \mu\text{m}) \dots\dots$	1.27	1.99	2.62	4.03	6.07	6.71	9.03
$n = 3, i = 45^\circ, T_{\text{eff}} = 30 \text{ kK}, R_{\text{out}} = 21.4 R_s, T_d = 1/2 T_{\text{eff}}$							
$E^*(V^* - H) \dots\dots$	0.02	0.03	0.06	0.30	0.91	1.08	1.65
$E^*(V^* - K) \dots\dots$	0.02	0.04	0.09	0.45	1.16	1.34	1.94
$E^*(V^* - 4.8 \mu\text{m})$	0.03	0.11	0.31	1.04	1.86	2.06	2.69
$E^*(V^* - 9 \mu\text{m}) \dots$	0.04	0.31	0.72	1.61	2.48	2.68	3.33
$E^*(V^* - 18 \mu\text{m})$	0.09	0.79	1.35	2.32	3.22	3.42	4.05
$R_d/R_s(H) \dots\dots\dots$	1.23	1.24	1.25	1.41	2.10	2.28	2.97
$R_d/R_s(K) \dots\dots\dots$	1.23	1.24	1.26	1.55	2.34	2.54	3.31
$R_d/R_s(4.8 \mu\text{m}) \dots$	1.24	1.27	1.39	2.17	3.15	3.44	4.56
$R_d/R_s(9 \mu\text{m}) \dots\dots$	1.24	1.39	1.79	2.76	4.07	4.49	6.06
$R_d/R_s(18 \mu\text{m}) \dots\dots$	1.26	1.86	2.46	3.75	5.67	6.25	8.48
$n = 3, i = 45^\circ, T_{\text{eff}} = 30 \text{ kK}, R_{\text{out}} = 14.6 R_s, T_d = 2/3 T_{\text{eff}}$							

Table 1—Continued

Parameter	1.0×10^{-12}	5.1×10^{-12}	1.0×10^{-11}	ρ_0 (g cm $^{-3}$) 3.1×10^{-11}	8.1×10^{-11}	1.0×10^{-10}	2.0×10^{-10}
$E^*(V^* - H)$	0.02	0.03	0.06	0.29	0.91	1.08	1.65
$E^*(V^* - K)$	0.02	0.05	0.12	0.60	1.38	1.57	2.18
$E^*(V^* - 4.8 \mu\text{m})$	0.02	0.11	0.31	1.04	1.86	2.06	2.67
$E^*(V^* - 9 \mu\text{m})$.	0.05	0.43	0.92	1.86	2.75	2.96	3.57
$E^*(V^* - 18 \mu\text{m})$	0.13	1.00	1.59	2.58	3.47	3.66	4.23
$R_d/R_s(H)$	1.23	1.24	1.25	1.42	2.10	2.29	2.97
$R_d/R_s(K)$	1.23	1.24	1.27	1.58	2.39	2.60	3.40
$R_d/R_s(4.8 \mu\text{m})$.	1.24	1.27	1.39	2.17	3.15	3.44	4.56
$R_d/R_s(9 \mu\text{m})$...	1.24	1.38	1.79	2.76	4.07	4.48	6.05
$R_d/R_s(18 \mu\text{m})$..	1.26	1.95	2.55	3.92	5.95	6.56	8.82

Table 2. Adopted Main Sequence Colors

T_{eff} (kK)	$V - K$ (mag)	$V - 9 \mu\text{m}$ (mag)	$V - 18 \mu\text{m}$ (mag)
10	−0.06	−0.07	−0.07
12	−0.23	−0.29	−0.29
14	−0.34	−0.43	−0.44
16	−0.43	−0.54	−0.55
18	−0.51	−0.64	−0.65
20	−0.58	−0.74	−0.75
22	−0.64	−0.82	−0.83
24	−0.70	−0.90	−0.91
26	−0.74	−0.96	−0.98
28	−0.79	−1.02	−1.03
30	−0.83	−1.07	−1.08

Table 3. Be Star Color Excesses

HD	$E^*(V^* - K)$ (mag)	$E^*(V^* - 9 \mu\text{m})$ (mag)	$E^*(V^* - 18 \mu\text{m})$ (mag)
144	0.05	0.12	...
4180	0.13	1.54	2.44
5394	0.54	1.83	2.51
6811	−0.34	−0.02	0.41
10144	0.03	0.29	0.43
10516	0.46	1.68	2.68
18552	0.11	0.74	1.62
20336	0.03	1.47	2.16
22192	0.33	1.75	2.62
23016	0.03	0.06	...
23302	−0.07	0.72	3.24
23480	−0.06	0.29	1.72
23552	−0.07	0.53	1.54
23630	0.29	0.28	0.97
23862	0.10	0.45	1.25
25940	0.08	1.16	1.99
28497	0.30	1.87	2.51
29866	0.03	0.72	1.49
30076	0.57	1.63	2.60
32343	0.39	1.21	2.43
32990	−0.05	0.07	...
32991	0.46	1.56	2.65
35439	−0.23	1.54	2.12
36576	0.70	1.88	2.95
37202	0.72	1.71	2.56
37490	−0.15	0.96	1.68
37795	0.10	0.51	1.30
41335	0.52	1.90	...
44458	−0.19	1.49	2.21
45542	0.00	0.32	0.89
45910	1.02	1.79	2.15
46860	0.06	0.13	...
50013	0.23	1.49	2.21
50123	0.90	1.60	2.08
50820	1.01	0.80	1.33
54309	0.39	1.00	1.90
56014	−0.04	0.88	1.40
56139	0.01	1.28	2.36
57150	0.40	1.67	2.52
57219	−0.06	0.12	...
58155	−0.04	0.00	...
58343	−0.25	...	2.19
58715	−0.03	0.47	1.17
60606	0.52	1.41	2.57
60855	0.75	...	3.09

Table 3—Continued

HD	$E^*(V^* - K)$ (mag)	$E^*(V^* - 9 \mu\text{m})$ (mag)	$E^*(V^* - 18 \mu\text{m})$ (mag)
63462	0.28	...	1.94
65875	0.39	1.73	2.64
66194	0.64	1.52	2.69
68980	0.48	1.62	2.45
71510	0.01	0.09	...
72067	−0.02	1.08	2.03
75311	−0.09	0.19	1.05
77320	0.39	1.16	1.41
79621	0.03	0.02	...
83953	0.50	...	2.37
86612	0.10	1.57	2.58
88661	0.54	1.78	2.69
91120	0.06	0.46	1.21
91465	0.32	1.51	2.23
105435	0.29	1.64	2.49
107348	0.03	0.55	...
109387	0.29	1.42	2.30
110432	0.26	1.82	2.50
113120	−0.44	1.33	2.09
120324	0.07	1.69	2.24
120991	0.29	0.07	1.03
121847	−0.03	0.00	...
124367	0.42	1.56	2.50
127972	0.10	1.13	1.87
137387	0.07	0.45	...
138749	−0.01	0.07	0.20
142184	0.09	0.54	1.18
142926	0.11	0.48	1.05
148184	0.49	1.93	2.71
153261	0.83	2.09	2.92
156325	0.00	0.12	...
157042	0.20	1.34	2.02
158427	0.64	...	2.48
158643	0.39	...	4.40
164284	−0.13	0.05	0.59
164447	−0.07	0.12	...
167128	0.03	0.62	1.34
168797	−0.02	0.24	...
170235	−0.13	0.07	...
171780	0.29	0.12	...
173370	0.04	0.26	0.28
173948	0.12	−0.03	0.23
174237	0.21	0.75	...
175869	0.03	0.06	...
178175	0.29	...	2.40

Table 3—Continued

HD	$E^*(V^* - K)$ (mag)	$E^*(V^* - 9 \mu\text{m})$ (mag)	$E^*(V^* - 18 \mu\text{m})$ (mag)
183362	0.55	1.77	...
185037	0.04	0.61	...
187567	0.56	1.78	2.63
187811	0.33	0.35	1.38
189687	0.04	0.33	1.46
191610	0.25	0.14	0.78
192044	0.12	0.81	1.37
193911	0.00	0.51	1.23
194244	0.04	0.24	...
194335	0.19	1.34	2.41
195554	0.03	0.17	...
196712	−0.04	0.53	...
197419	0.28	0.88	...
198183	−0.09	−0.08	0.28
199218	0.08	0.84	...
200120	0.45	1.69	2.13
200310	−0.03	0.26	1.79
202904	0.04	1.62	2.50
203025	−0.32	−0.12	...
203467	0.58	1.91	3.47
205551	−0.14	0.06	...
205637	0.14	0.69	1.37
208057	−0.06	0.03	...
208682	−0.28	−0.14	...
209014	0.04	0.62	1.32
209409	0.22	1.10	1.94
209522	−0.01	−0.06	...
210129	−0.09	1.24	1.99
212076	0.41	1.74	2.48
212571	−0.41	0.51	0.91
214168	0.25	0.62	...
214748	−0.02	0.14	0.99
216057	−0.07	0.01	...
216200	0.25	0.63	...
217050	0.28	1.65	2.58
217543	−0.07	0.33	...
217675	−0.12	0.04	0.44
217891	−0.05	0.93	1.58
224544	0.00	−0.07	...
224559	0.10	1.52	2.15

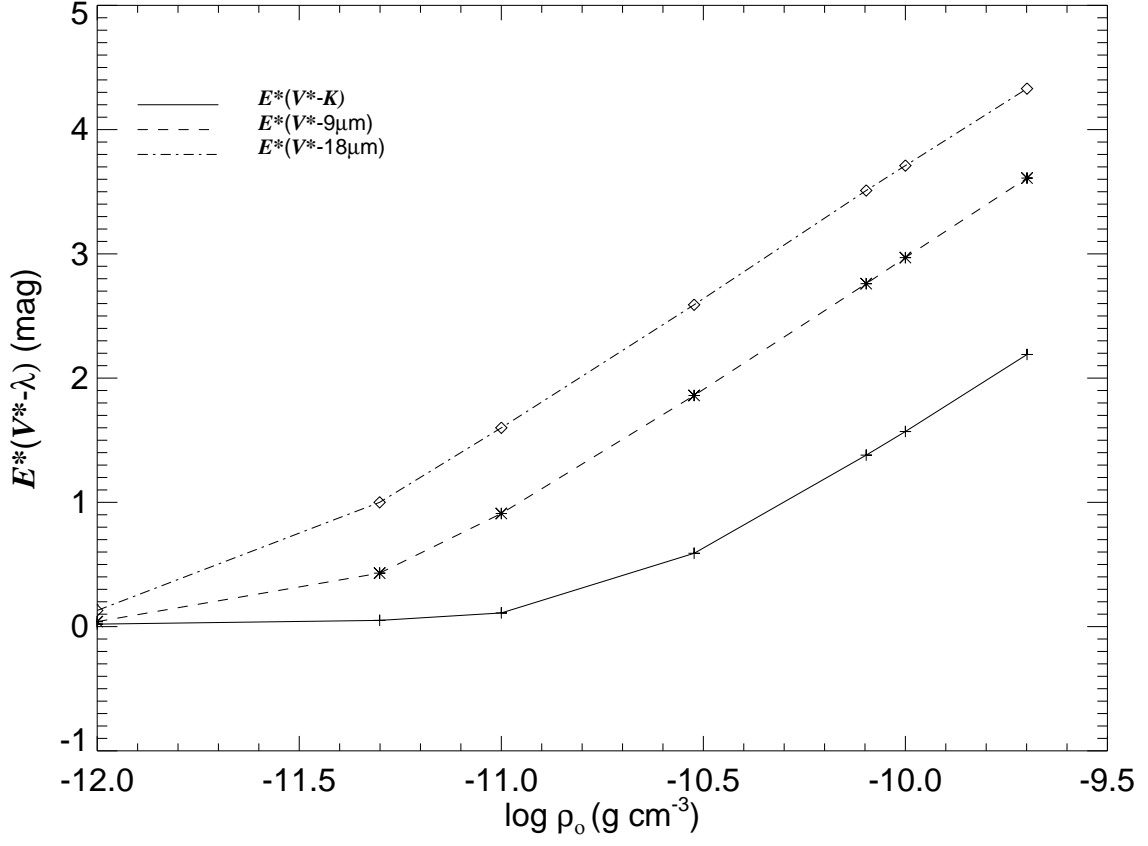


Fig. 1.— Plots of the variation in color excess as function of disk base density for the default model parameters ($n = 3$, $i = 45^\circ$, $T_{\text{eff}} = 30$ kK, $R_{\text{out}} = 21.4R_s$, $T_d = 2/3T_{\text{eff}}$). The excess emission increases with increasing disk base density ρ_0 and wavelength.

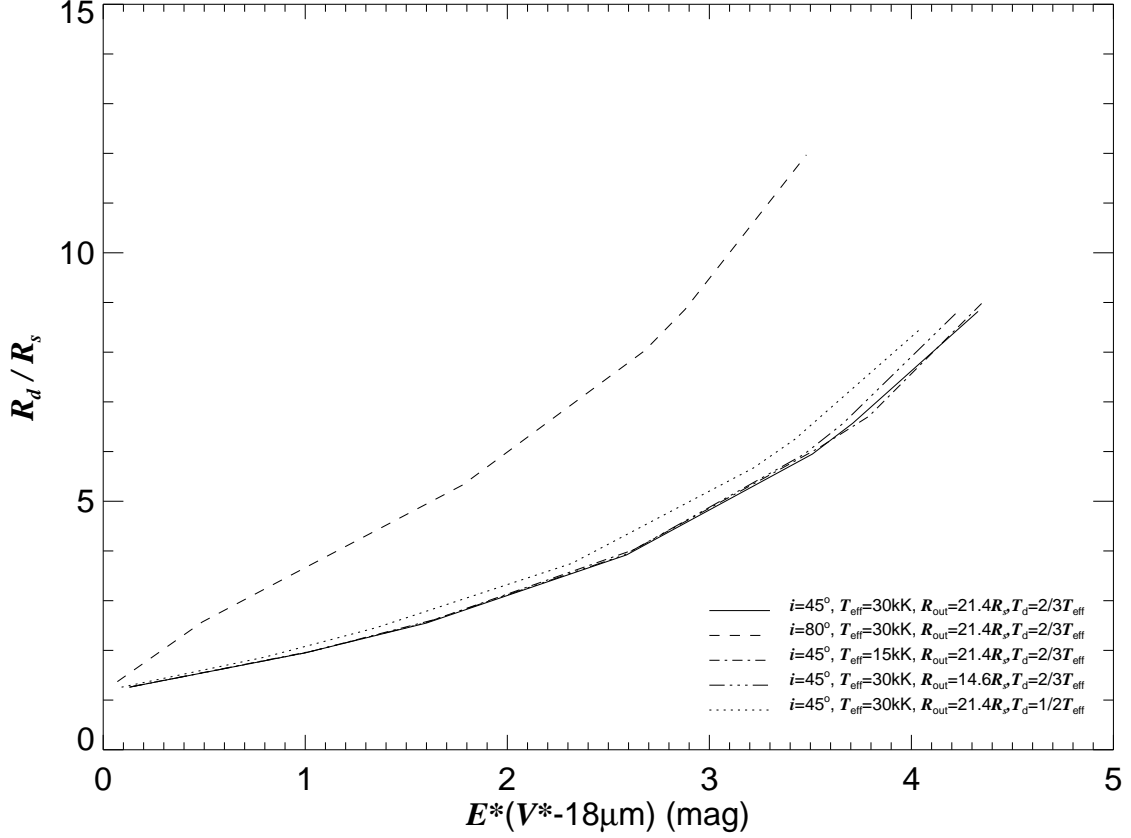


Fig. 2.— Plots of the ratio of disk HWHM radius to stellar radius as a function of the flux excess at $18 \mu\text{m}$. The solid line illustrates the relationship for the default model while the other line styles show the results found by changing one of the model parameters (indicated in the legend).

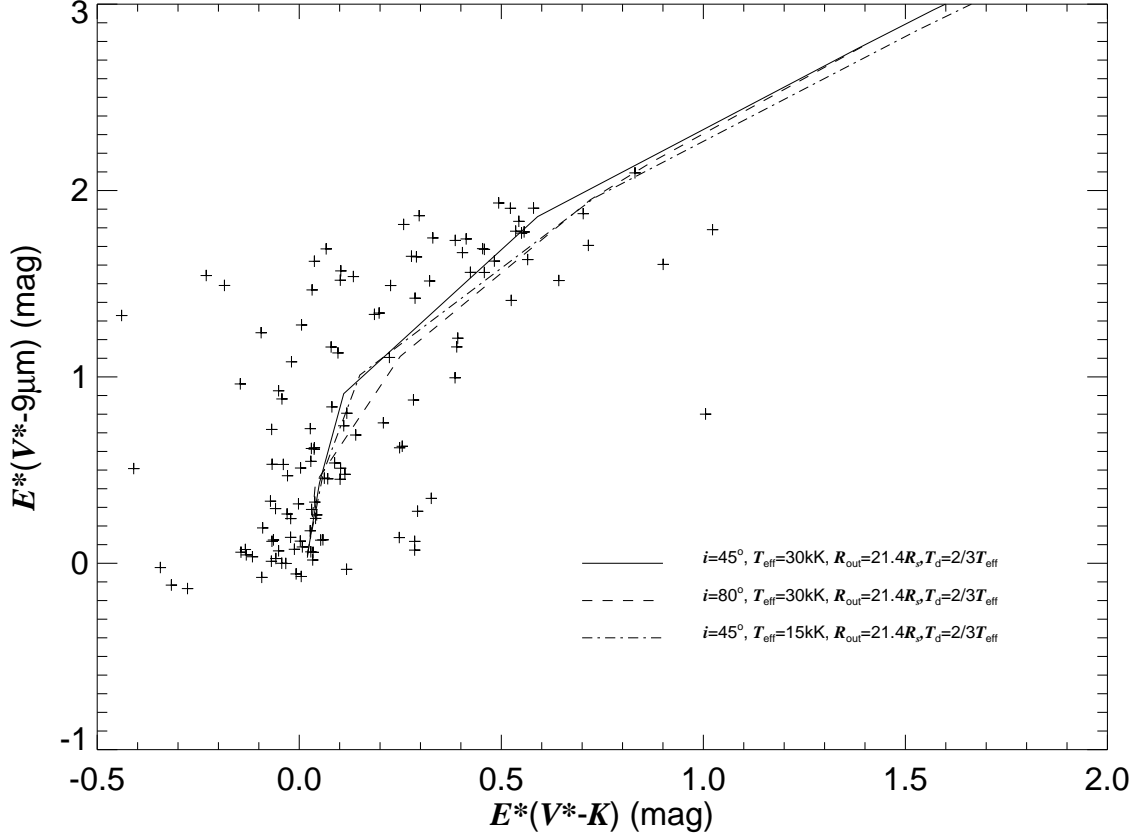


Fig. 3.— A color excess – color excess diagram showing the $9 \mu\text{m}$ flux excess as a function of the K_s -band excess. The solid line shows our results using the default model input parameters, the dashed line represent a model with a high-inclination disk ($i = 80^\circ$), and the dashed-dotted line shows the case of a cooler Be star ($T_{\text{eff}} = 15 \text{ kK}$). The plus signs indicate the observed excesses of Be stars derived from 2MASS and AKARI/IRC photometry.

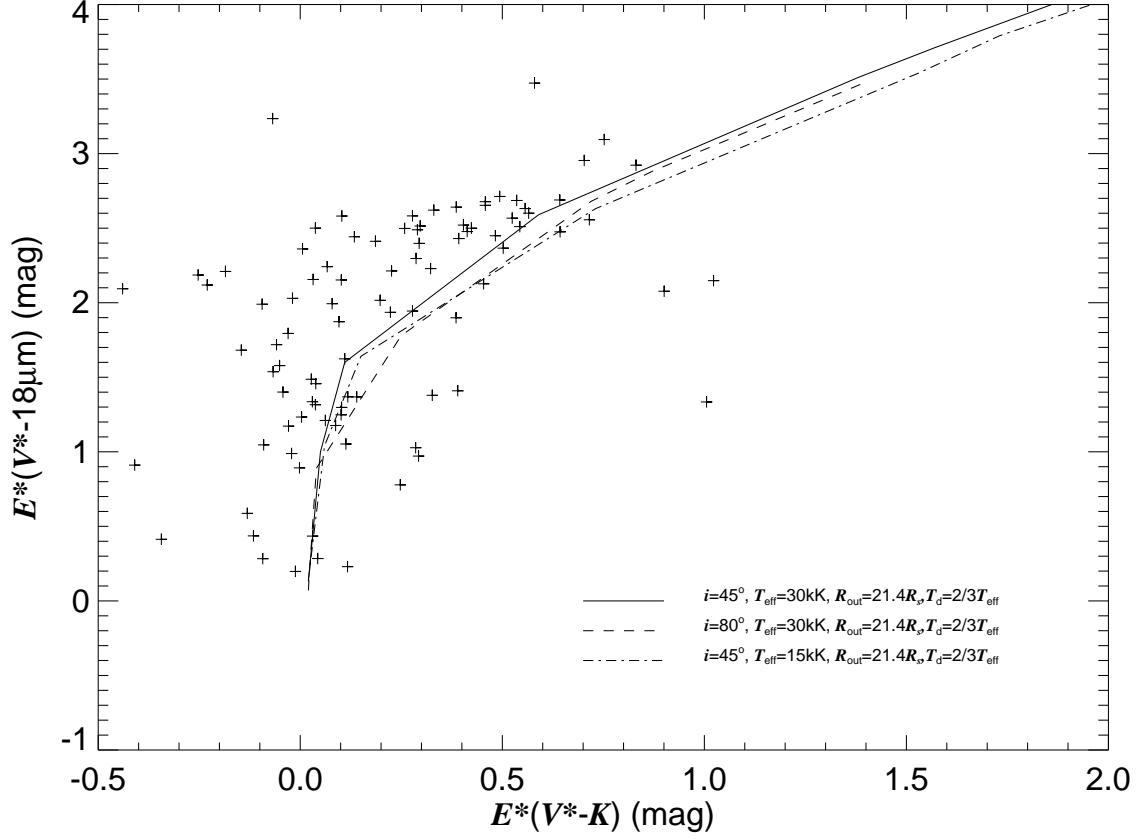


Fig. 4.— A color excess – color excess diagram showing the $18\ \mu\text{m}$ flux excess as a function of the K_s -band excess (in the same format as Fig. 3).

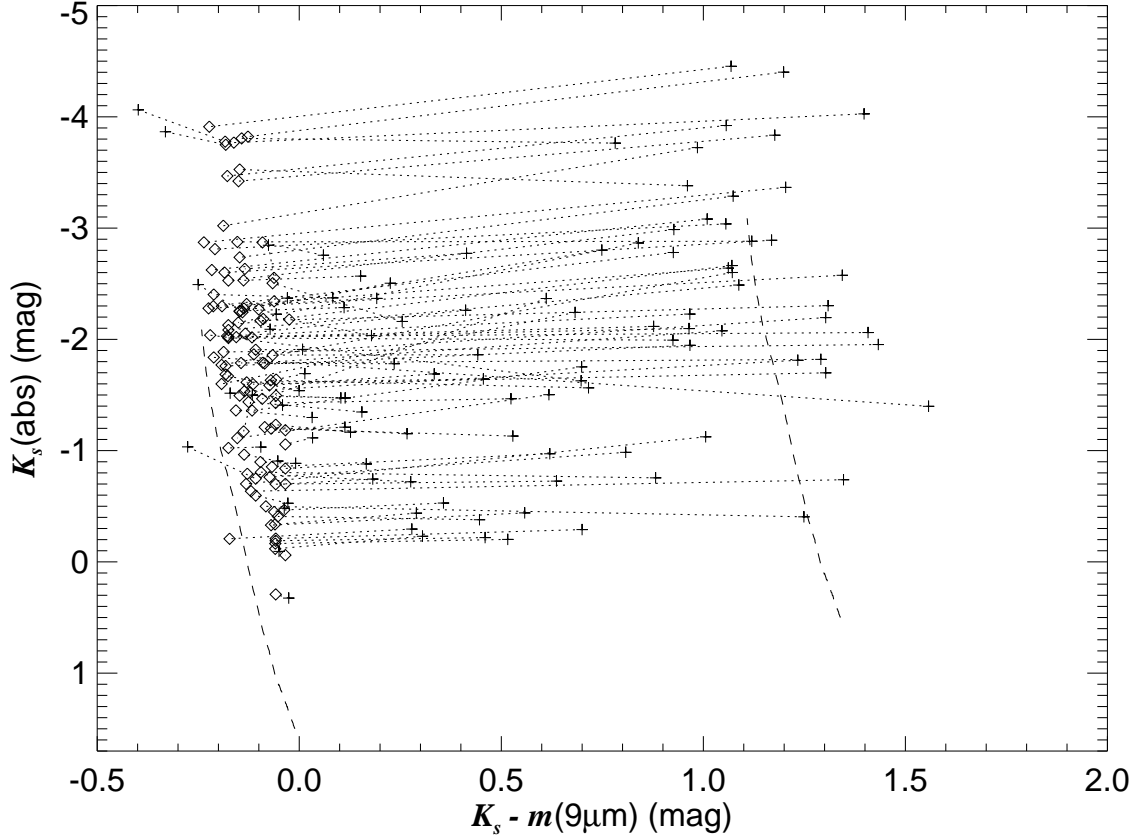


Fig. 5.— A color – magnitude diagram showing the absolute K_s magnitude corrected for interstellar extinction as a function of the interstellar reddening corrected, color index $K_s - m(9 \mu\text{m})$ for our Be star sample (shown as plus signs). Each target point is connected by a dotted line to a diamond representing the color and magnitude of the B star alone. The left dashed line represents the zero-age main-sequence for stars with $T_{\text{eff}} = 10 - 30 \text{ kK}$, and this also is shown translated in color and magnitude for a dense disk as the dashed line on the right hand side.

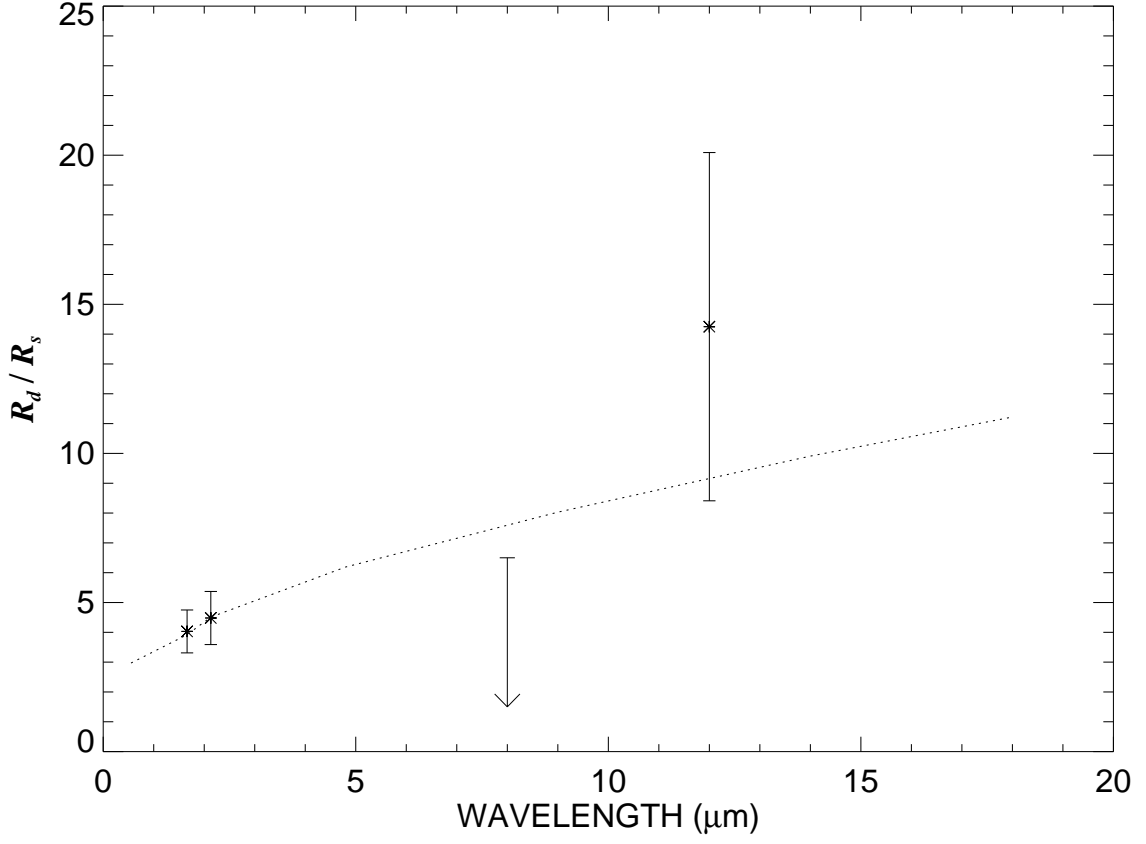


Fig. 6.— The disk-to-stellar radius ratio as a function of wavelength for our model of the Be star ζ Tau (dotted line). Also shown are the measured sizes from interferometry (or upper limit on the size for the 8 μm observation) based on an adopted stellar angular diameter of 0.40 mas.